Nonnative interactions regulate folding and switching of myristoylated protein

Dalit Shental-Bechor[a,1], Martin T.J. Smith[b,1], Duncan MacKenzie[b], Aron Broom[b], Amir Marcovitz[a], Fadila Ghashut[b], Chris Go[b], Fernando Bralha[b], Elizabeth M. Meiering[b,2], and Yaakov Levy[a,2]

[a]Department of Structural Biology, Weizmann Institute of Science, Rehovot 76100, Israel; and [b]Department of Chemistry, Guelph-Waterloo Centre for Graduate Work in Chemistry and Biochemistry, University of Waterloo, Waterloo, ON, Canada N2L 3G1

Edited by Peter G. Wolynes, Rice University, Houston, TX, and approved June 19, 2012 (received for review April 7, 2012)

We present an integrated experimental and computational study of the molecular mechanisms by which myristoylation affects protein folding and function, which has been little characterized to date. Myristoylation, the covalent linkage of a hydrophobic C14 fatty acyl chain to the N-terminal glycine in a protein, is a common modification that plays a critical role in vital regulated cellular processes by undergoing reversible energetic and conformational switching. Coarse-grained folding simulations for the model pH-dependent actin- and membrane-binding protein hisactophilin reveal that nonnative hydrophobic interactions of the myristoyl with the protein as well as nonnative electrostatic interactions have a pronounced effect on folding rates and thermodynamic stability. Folding measurements for hydrophobic residue mutations of hisactophilin and atomistic simulations indicate that the nonnative interactions of the myristoyl group in the folding transition state are nonspecific and robust, and so smooth the energy landscape for folding. In contrast, myristoyl interactions in the native state are highly specific and tuned for sensitive control of switching functionality. Simulations and amide hydrogen exchange measurements provide evidence for increases as well as decreases in stability localized on one side of the myristoyl binding pocket in the protein, implicating strain and altered dynamics in switching. The effects of folding and function arising from myristoylation are profoundly different from the effects of other post-translational modifications.

coarse-grained simulation | funnel landscape | β-trefoil

Protein folding is governed by various physicochemical forces that bias the native state, which for many proteins is also the functional state, over the many alternative nonnative states. The network of native interactions has been found in many cases to be sufficient to capture the folding mechanism and kinetics of proteins (1, 2). The discrimination between native and nonnative interactions is the foundation of the principle of minimal frustration (3) and explains the power of native topology-based models in studying folding biophysics (4). The dominant role of native interactions is manifested by the funnel-shaped energy landscape for folding that suggests folding is robust and an efficient process. The information stored in the native topology may, however, be tuned by various factors such as confining the protein in a small space, crowding agents, or conjugating the protein to other biomolecules [e.g., oligosaccharides (5) or fatty acyl chains such as myristoyl (6)]. In addition to manipulating folding characteristics by modifications or environmental conditions, nonnative interactions, which are by definition in conflict with the native state, may decorate the folding funnel (7, 8) by increasing energetic frustration (9) between interactions and therefore landscape roughness. The degree of roughness, which affects the trapping of the protein in nonnative states, depends on the particular sequence of the protein and can be tuned by mutations.

Investigations of several proteins have reported evidence for nonnative interactions that assist, rather than hinder, folding (10–14), and more importantly they may also support function (6, 15, 16) by assisting conformational changes. Residues in functional sites in proteins have been implicated in causing geometric frustration (17) or increasing localized energetic frustration (16). Nonnative interactions that result with localized frustration can transiently be formed, for example, between hydrophobic residues (13) or between oppositely charged residues (18–20). This is akin to frustration in RNA folding that arises from negatively charged groups (21). The formation of nonnative interactions may affect folding in various ways. For example, nonnative interactions in the unfolded state may affect its entropy and therefore the overall stability of the protein. Also, nonnative interactions in the transition state that support the critical nucleus may speed up the folding process.

In the current study, we investigate the effect of myristoylation on protein folding and in particular the involvement of nonnative interactions. Myristoylation is a common modification, where a saturated C14 fatty acyl chain is covalently linked to the N-terminal glycine in a protein (22). In many proteins the myristoyl interconverts between a sequestered state, where it is located in a hydrophobic binding pocket, and an accessible state, where it is available to bind to membrane or other proteins. Often this interconversion, or switching, is reversible and controlled by the binding of ligand. Myristoyl switching is associated with diverse and vital regulated signaling pathways in cells (22).

We investigate here the effect of myristoylation on the folding kinetics and thermodynamics of the β-trefoil protein, hisactophilin, a small (118 residues) protein from *D. discoideum* (Fig. 1*A*). The function of hisactophilin is to reversibly recruit actin filaments to membranes during chemotaxis and osmotic stress. Previous studies revealed that increasing hisactophilin charge with decreasing pH favors actin and membrane binding but decreases protein stability and folding kinetics (23, 24). The myristoyl increases hisactophilin stability with an apparent pK_a of 6.95 as it switches between a "sequestered" state at high pH, where the myristoyl is buried in the protein core (Fig. 1*A*), and an "accessible" state at low pH for membrane binding (6). Concomitantly, the myristoyl markedly accelerates both folding and unfolding kinetics, and undergoes rapid native-state switching, implicating the long and flexible hydrophobic myristoyl chain in creating strain in the native state and forming nonnative interactions during folding and switching. Here we report an integrated approach combining various computational and experimental methods to analyze myristoylated hisactophilin, including characterization of hydrophobic mutations distributed in the primary and tertiary structure of the protein (Fig. 1*B*). Variants include a triple

Author contributions: D.S.-B., M.S., D.M., A.B., E.M.M., and Y.L. designed research; D.S.-B., M.S., D.M., A.B., A.M., F.G., C.G., and F.B. performed research; D.S.-B., M.S., D.M., A.B., A.M., E.M.M., and Y.L. analyzed data; and D.S.-B., M.S., D.M., A.B., E.M.M., and Y.L. wrote the paper.

The authors declare no conflict of interest.

This article is a PNAS Direct Submission.

[1]D.S.-B. and M.S. contributed equally to this work.

[2]To whom correspondence may be addressed. E-mail: koby.levy@weizmann.ac.il or meiering@uwaterloo.ca.

This article contains supporting information online at www.pnas.org/lookup/suppl/doi:10.1073/pnas.1201803109/-/DCSupplemental.

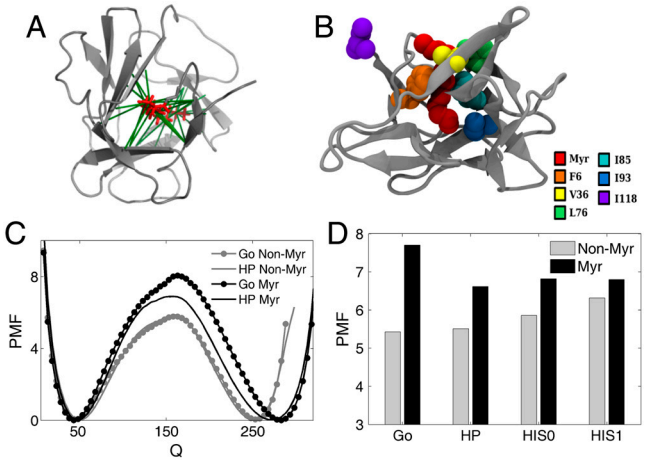

Fig. 1. The effect of nonnative interactions on simulating the folding of nonmyristoylated and myristoylated hisactophilin. (*A*) Top view of myristoylated hisactophilin (backbone in grey cartoon) with native contacts (green) between the myristoyl group (red) and the protein. (*B*) Side view of hisactophilin with space-filling representations for mutated residues. (*C*) Potential of mean force vs. Q, the number of native contacts within hisactophilin, for folding of myristoylated (black) and nonmyristoylated (grey) hisactophilin calculated for four different simulation models: the native topology-based model (Go), nonnative hydrophobic model (HP), charged residue model at high pH (His0), and positively charged histidine at low pH electrostatic model (His1). The His0 and His1 electrostatic models also include the HP model. Folding barriers are calculated at the folding temperature, T_F. (*D*) The folding barrier for nonmyristoylated (grey) and myristoylated (black) hisactophilin at the T_F of each system.

myristoyl binding pocket mutant (F6L/I85L/I93L) in which pH-dependent switching is abolished (25), and single mutations that alter stereochemistry (I85L) or truncate side chains inside (V36A and L76A) or outside (I118A) the binding pocket. The results provide unique insight into the role of nonnative interactions in folding as well as the atomistic mechanism of myristoyl switching.

Results and Discussion

Hydrophobic and Electrostatic Nonnative Interactions are Necessary to Accurately Simulate the Folding of a Myristoylated Protein. We first simulated the folding of hisactophilin in its nonmyristoylated form using the native topology-based (Go) model that considers only native interactions found in the high-resolution structure of the protein (Fig. 1*C*, *SI Results*). For hisactophilin, we observed two-state folding with a relatively high energy barrier (5.9 kT) (Fig. 1*C*) consistent with experimentally observed relatively slow folding (24). While the native topology-based model captures many features of the folding energy landscape, it neglects the roughness of the landscape due to nonnative interactions, which surely exist to some extent. Nonnative interactions may transiently form in either the unfolded state or the transition state and influence both folding thermodynamics and kinetics. We then modeled potential nonnative interactions by the formation of nonspecific interactions between hydrophobic residues (HP model) as well as electrostatic nonnative interactions among Asp, Glu, Lys, and Arg residues (model His0) and with positively charged histidines (model His1) (Fig. 1*D*, *SI Results*).

The modeling is consistent with experimentally observed large decreases in hisactophilin folding rate with decreasing pH (19, 24).

We then studied the effect of the myristoyl group on folding kinetics using a coarse-grained simulation. The energy barrier at T_F was increased from 5.4 kT to 7.7 kT due to myristoylation. Adding the hydrophobic nonnative interactions between the myristoyl group and the protein resulted in a dramatic acceleration of folding and a decrease in the energy barrier to 6.6 kT (Fig. 1*D* and Fig. S1). Note that the energy barrier of the myristoylated protein is higher than that of the nonmyristoylated protein (even when the hydrophobic nonnative interactions are included), because the barrier heights were estimated at T_F of each system. When, however, the folding barrier heights were measured at the same temperature for all the systems, the experimentally observed accelerated folding upon myristoylation is reproduced. Integration of electrostatic nonnative interactions (at low and high pH) within the myristoylated protein did not have an additional effect on the energy barrier. From examination of the distances between residues and the change in distances upon integration of the various nonnative interactions we conclude that the major effect on the folding is in the transition state ensemble. Hydrophobic nonnative interactions position the myristoyl group 15 Å closer to the other hydrophobic residues in the protein with respect to the native topology-based simulations that included only native interactions (Fig. S2). The electrostatic interactions, especially at high pH, had a dual effect on the distances; the nonpolar residues were still closer but the His residues were slightly farther from one another. It is possible that simulations at different ionic strength would also affect electrostatic interactions and therefore folding, as shown for RNA folding (26). The incorporation of the nonnative interactions (both hydrophobic and electrostatic) also influences the thermal stability of the protein as measured by the simulation, with a pH-dependence that is consistent with experiment (6, 23) (*SI Results*).

To better understand the effect of the myristoylation on the kinetics and stability of the protein, we gradually changed the strength of the native and nonnative interactions between the myristoyl group and the protein. To this end, we gradually changed the value of ε and κ—which correspond to the strength of native and nonnative contacts, respectively—formed between the myristoyl group and the relevant amino acids. When ε equals unity, the contacts between the myristoyl group and the protein are equivalent in their energy contribution to the rest of the contacts within the protein. On the other hand, when ε equals zero, these contacts do not make any enthalpic contribution. The contacts between the myristoyl and the protein are shown in Fig. 1*A*. The matrix in Fig. 2*A* presents variation in the T_F of myristoylated hisactophilin for different values of κ and ε. In general, the T_F is increased (i.e., the protein is more thermostable) as ε and κ are increased, probably because more interactions are formed between the myristoyl and the protein and because the enthalpy is larger. Calculation of the average radius of gyration for the protein, $\langle Rg \rangle$, shows that the folded state is mostly affected by variations in the strength of ε and κ while the $\langle Rg \rangle$ of the unfolded state is robust (Fig. S3). We therefore conclude that the major effect on the free energy is on the folded state. The changes in the dimensions of the folded state are in agreement with changes in the enthalpy and entropy of the folded state. The more compact folded state with increased κ and ε has correspondingly lower enthalpy and lower entropy, which results in an overall decrease in the free energy of the folded state. It is notable that the strength of nonnative interactions in the simulations seems to have an effect on both the native and the transition state. The nonnative interactions in the native state may represent interactions involved in switching.

Analysis of Myristoyl Interactions in the Transition State and the Native State. Fig. 2*B* presents a summary of the folding energy barrier of the myristoylated protein for differing strengths of native and nonnative interactions. The matrix illustrates that the energy barrier for folding increases with the value of ε—i.e., when the myristoyl is forced to be sequestered in the protein (and interacts strongly with its pocket). When hydrophobic nonnative interactions are included, the energy barrier may be significantly decreased, in accordance with the experimental finding that the nonnative interactions play a role in accelerating folding kinetics of the myrisoylated hisactophilin (6). Notably, the increase in the

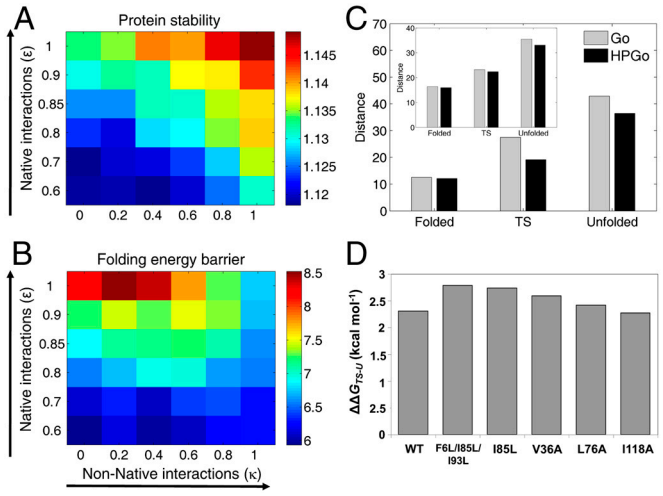

Fig. 2. Interplay between nonnative interactions on the folding barrier and stability. (*A*) The value of the folding temperature, T_F, at different strengths of native (ε) and nonnative (κ) interactions between the myristoyl and the protein. (*B*) The value of the free energy barrier for folding at different values of ε and κ (at T_F). In these simulations, the ε of the protein contacts equals 1. $\kappa = 0$ corresponds to the pure native topology-based model. (*C*) The median of the distances of all the hydrophobic nonnative pairs between the protein and the myristoyl in the folded-, unfolded-, and transition-state ensembles for the native topology-based model (Go, grey) and the model supplemented by nonnative hydrophobic interactions (HPGo, black). The *inset* shows the median of all hydrophobic nonnative interactions within the protein. (*D*) The decrease in the energy barrier for folding of WT and mutant hisactophilin upon myristoylation, $\Delta\Delta G_{TS\text{-}U} = m_{f,\mathrm{avg}} \cdot [(\mathrm{urea})_{\ln(kf)=0,\mathrm{myr}} - (\mathrm{urea})_{\ln(kf)=0,\mathrm{nonmyr}}]$, calculated using the average denaturant dependence for $\ln(k_f)$, $m_{f,\mathrm{avg}}$, for all the variants (Fig. S4).

energy barrier is significantly moderated when the nonnative interactions are included ($\kappa = 1$) compared to when they are omitted ($\kappa = 0$). The formation of the hydrophobic nonnative interactions at the folding transition state is illustrated by shorter pairwise distances between hydrophobic residues. These distances in the transition state ensemble are generally shorter for nonnative interactions between the myristoyl and hydrophobic residues than between two hydrophobic residues (Fig. 2*C*).

Experimental measurement of folding kinetics for hisactophilin variants can provide information on the formation of interactions for specific groups (e.g., myristoyl and/or amino acid sidechains) during protein folding. As mentioned above, such measurements have shown that the myristoyl group greatly accelerates the folding of wild-type (WT) hisactophilin and that this involves the formation of nonnative interactions in the transition state (6). The effects of mutations (Fig. 1*B*) that abolish switching [e.g., F6L/I85L/I93L (25) and I85L, *vide infra*] and truncate hydrophobic residues inside and outside the myristoyl binding pocket (V36A, L76A, and I118A) range from slightly increasing to considerably decreasing the folding rate (Fig. S4). Remarkably, however, the large increase in folding rate conferred by myristoylation remains largely unchanged for all mutants (Fig. 2*D*). In other words, none of the mutated residues appear to make critical, specific interactions with the myristoyl group in the transition state ensemble. This suggests that the myristoyl group accelerates the rate of folding by making nonspecific, including nonnative, interactions in the transition state. These interactions may be highly robust to mutation and have the effect of smoothing the folding energy landscape and reducing frustration.

Energetic Myristoyl Switch with pH. Experimental studies of hisactophilin show a clear energetic switch in the myristoylated relative to nonmyristoylated form upon changing from low to high pH (6). At low pH, in excess ligand (H^+) the stabilization upon myristoylation is much smaller than at high pH, where the absence of bound H^+ differentially increases the stability of both the myristoylated and nonmyristoylated protein (Fig. 3*A*). Assuming that the change in pH mostly affects the protonation state of histidine residues, we simulated the protein using the His0 and His1 models (which model the protein at high and low pH, respectively). In the simulations the myristoylated protein is more stable than the nonmyristoylated protein both at low and high pH (Fig. 3*B*), similar to experiment. However, the modulation of the stabilization with pH could not be simply observed in the simulations, but only by assuming that the strength of the interactions of the myristoyl with the protein (either native or nonnative) is indirectly affected by the pH due to the change in the histidine protonation state. This energetic switch is accompanied by a conformational switch: at low pH the myristoyl group is in the accessible state and at high pH it is sequestered. We observe this dual effect of energetic and structural switching when we manipulate the strength of the native or nonnative interactions between the myristoyl group and the protein. In this way, we can decrease the amount of extra stability that was achieved by adding the myristoyl, implying that changes in pH not only affect the protonation state of the histidine residues, but also change the strength of the interactions between the protein and the myristoyl. We conjecture, therefore, that the switch originates from a thermodynamic effect. In the absence of ligand (at high pH), the protein is thermodynamically stable and undergoes minor structural fluctuations; therefore the probability of the switching between the sequestered and accessible states is low (high free energy). In excess of ligand (at low pH), the protein is less stable, the probability for the switching is higher, and the accessible state is more populated. This leads to a lower thermodynamic stability due to the loss of enthalpic contributions from the direct interaction of the myristoyl and the hydrophobic pocket. Thus, simulations provide evidence that the experimentally observed energetic switch is governed by the balance of native and nonnative interactions. This highlights the importance of modeling nonnative interactions for understanding the mechanism of myristoyl switching.

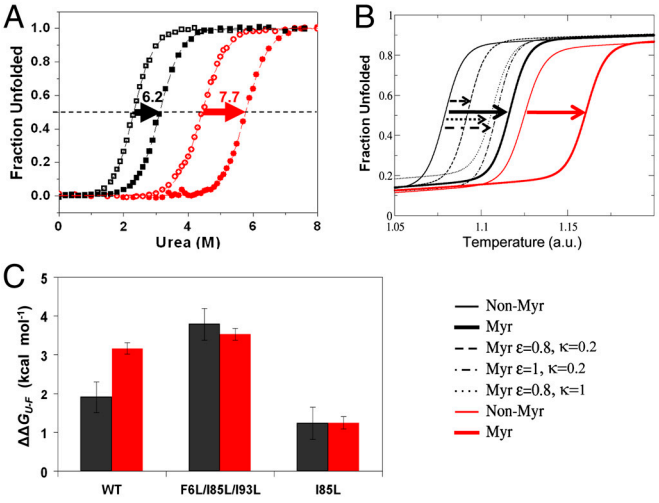

Fig. 3. Energetics of myristoyl switching. (*A*) Equilibrium urea denaturation curve measurements of stability for nonmyristoylated (open symbols) and myristoylated (closed symbols) hisactophilin at pH 6.2 (black squares) and 7.7 (red circles). Stabilization upon myristoylation, $\Delta\Delta G_{U\text{-}F} = \Delta C_{\mathrm{mid}} \cdot m_{\mathrm{avg}}$, calculated from the difference in the midpoint of denaturation, ΔC_{mid}, for myristoylated relative to nonmyristoylated hisactophilin multiplied by m_{avg}, the average denaturant dependence of $\Delta G_{U\text{-}F}$ for the 2 forms of hisactophilin (6). (*B*) Simulated fraction unfolded vs. temperature for myristoylated (solid bold line) and nonmyristoylated (solid line) hisactophilin at low pH (black) and high pH (red) under different strengths of ε (native) and κ (nonnative) myristoyl interactions. (*C*) Stabilization upon myristoylation, $\Delta\Delta G_{U\text{-}F}$, for WT, F6L/I85L/I93L, and I85L hisactophilin at pH 6.2 (black) and pH 7.7 (red).

We then analyzed the contributions of individual residues to switching, using a combination of experimental measurements and atomistic simulations for mutant proteins. In previous experiments, we found that the switch in hisactophilin is broken in the triple myristoyl binding pocket mutant, F6L/I85L/I93L, such that the myristoyl group remains in the sequestered state and does not switch to the accessible state with decreasing pH (25) (Fig. 3*C*). We now report that the single mutation, I85L, breaks the switch in the opposite way—i.e., by weakening interactions of the myristoyl with the protein such that the mutant protein remains in the accessible state. It is noteworthy that this highly conservative mutation, changing only the stereochemistry of a single sidechain, essentially abolishes switching. We speculate that moving the branch point in the sidechain from the β- to the γ-carbon may create steric clashes with the myristoyl, interfering with it adopting its fully sequestered conformation, and concomitantly increasing protein dynamics such that coupling between the myristoyl binding pocket and sites of protonation is disrupted.

The F6L/I85L/I93L and I85L mutations have dramatically different effects on the transition state compared to the native state. Rather counterintuitively, despite the broken switching, both F6L/I85L/I93L and I85L fold slightly faster than WT in the myristoylated form (Fig. S4*A*). This suggests that the folding of the WT protein is slightly slowed—i.e., frustrated—by residues required for switching functionality. Nevertheless, as mentioned above, the energetics of the transition state relative to the unfolded state are robust (Fig. 2*D*). In contrast, the energetics of the native state and protein function are dramatically affected by the mutations (Fig. 3*C*). This suggests that I85L introduces too much strain into the native state to allow for switching, while F6L/I85L/I93L causes too large a reduction in strain, consistent with altered dynamics observed in atomistic simulations (*vide infra*).

Structural Switch of the Myristoyl among Sequestered, Accessible, and Exposed States. From our folding simulations, we identified the conditions where myristoyl switching occurs. Fig. 4*A* shows a two-dimensional free energy surface for the coupling between folding of hisactophilin (depicted by Q_{Folding}) and switching of the myristoyl group (depicted by $Q_{\text{Prot-Myristoyl}}$) for three sets of ε– and κ-parameters for native and nonnative interactions, respectively, of the myristoyl group. At low values of Q_{Folding}, the protein is unfolded and the myristoyl is highly exposed to solvent (i.e., $Q_{\text{Prot-Myristoyl}}$ is low but some sporadic interactions between the myristoyl and the protein are found). At high values of Q_{Folding}, the protein is folded and the myristoyl forms many more contacts with the protein as it fits in the hydrophobic pocket. When $\varepsilon = 0.6$ and $\kappa = 0$, the enthalpic stabilization is insufficient for populating the sequestered state. However, increasing the strength of the native and nonnative interactions ($\varepsilon = 0.8$ and $\kappa = 0.2$) results in the full insertion of the myristoyl into its pocket. The switching of the myristoyl from the exposed to the sequestered state follows the folding of the protein (Fig. 4*A*). Only when the strength of the interactions of the myristoyl with the protein are sufficiently strong (close to unity), a coupling between folding and switching emerges (i.e., the folding follows more two-state rather than three-state behavior). In this scenario, the strong coupling between folding and switching can be reduced when the strength of nonnative interactions is increased, as they may allow the protein to populate states other than the fully sequestered state while the rest of the protein is folded.

To further elucidate the switching mechanism, we analyzed the position of the tip of the myristoyl with respect to the bottom of its hydrophobic pocket; specifically, we measured the distance between the bead representing C13 and C14 of the myristoyl group and the center of mass of the beads representing the alpha carbons of three residues at the bottom of the barrel (V21, V61, and V101). This analysis revealed three typical structural states of the myristoyl group relative to the protein. The two limiting states correspond to the myristoyl being fully sequestered in the protein binding pocket versus the fully solvent exposed state of the myristoyl (states I and III in Fig. 4). In the remaining state, the myristoyl is partially accessible to the solvent (state II) and is stabilized by nonnative hydrophobic interactions with residues located at the rim of the pocket (Fig. 4*E*). This intermediate state (state II, in which the myristoyl forms about 8 native interactions with the protein compared to 25 in the fully sequestered state, Fig. 4*B*) resembles the accessible state that was observed in experiments as pH was lowered. In this accessible state, the

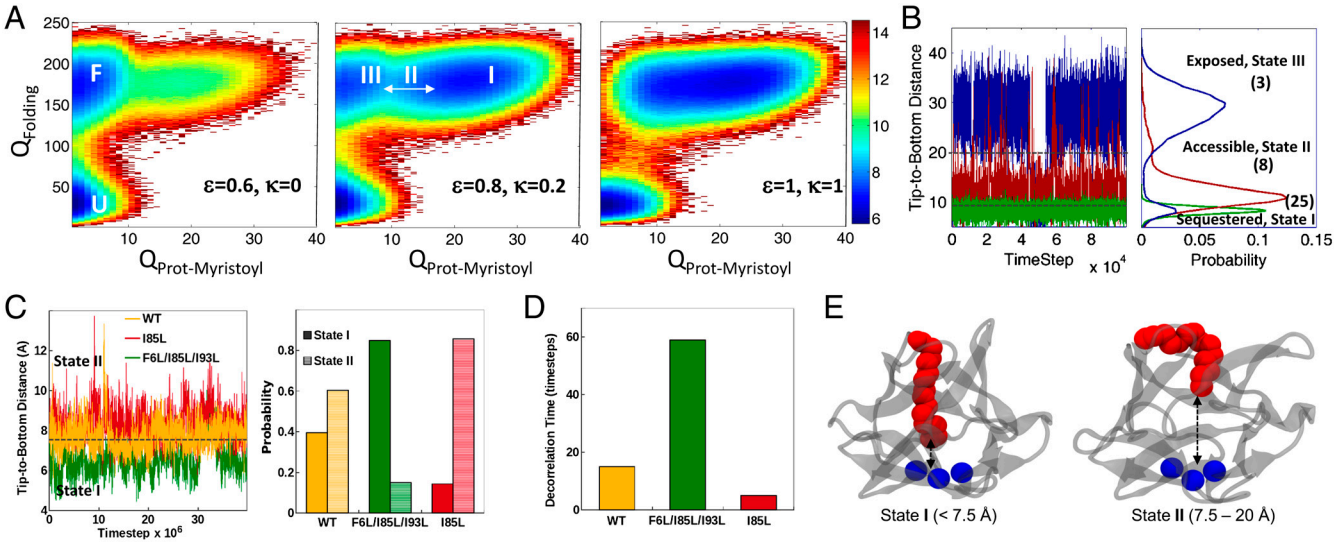

Fig. 4. Structural characterization of the myristoyl switching mechanism. (*A*) The coupling between folding and switching is shown by projecting the free energy onto two reactions coordinates: Q_{Folding} (number of native contacts within hisactophilin) and $Q_{\text{Prot-Myristoyl}}$ (number of native contacts between the myristoyl and hisactophilin) for $\varepsilon = 0.6$, $\kappa = 0$; $\varepsilon = 0.8$, $\kappa = 0.2$; and $\varepsilon = 1$, $\kappa = 1$. Blue and red areas correspond to highly and poorly populated states, respectively (free energy in units of kT). (*B*) Definition of the three states of the myristoyl relative to the bottom of the barrel: fully sequestered (state I, <7.5 Å), accessible (state II, 7.5–20 Å), and exposed (state III, >20 Å). The numbers in brackets refer to the average $Q_{\text{Prot-Myristoyl}}$ in each state. The blue, red, and green trajectories were simulated using different values of [ε, κ] which equal [0.6, 0], [0.8, 0.2], and [1.0, 1.0], respectively. (*C*) Analysis of atomistic molecular dynamics simulations for WT, F6L/I85L/I93L, and I85L showing effects of mutations on the probability of populating states I and II. (*D*) Decorrelation time of the tip-to-bottom distance. (*E*) Representative conformations of the myristoyl for states I and II that were found in atomistic simulations.

myristoyl group is less buried; however, there remain significant interactions between the myristoyl and the protein, based on measurements of energetics and NMR data (6).

In the simulations, the strength of native and nonnative interactions between the protein and the myristoyl has a major impact on the position of the myristoyl with respect to the protein. In general, we see that when the native interactions are strong ($\varepsilon \geq 0.9$), the protein is mostly in the sequestered state (state I) regardless of the strength of the hydrophobic nonnative interactions. The exposed state (state III) is common in simulations in which both the native and nonnative interactions are weak (κ and $\varepsilon < 0.6$). The partially accessible state (state II) is most common when the nonnative interactions are strong ($\kappa = 1$), but native contacts between the myristoyl and the pocket are weak ($\varepsilon < 0.7$, Fig. 4*A* and Fig. S5). Based on previous analyses of the pH dependence of stability and NMR data, switching from the sequestered state to the accessible state is caused by the binding of approximately 1.5 protons by a small number of histidine residues localized on one side of the protein (6, 25). Also, the protonation of the histidines is coupled to the state of nearby hydrophobic residues including F6, I85 and I93, which sensitively communicate pH changes to the myristoyl binding pocket as evidenced by switching being abolished in the F6L/I85L/I93L (25) and I85L (Fig. 3*C*) mutants. Therefore, we speculate that in hisactophilin at low pH, where the accessible state is favored, the nonnative interactions between the protein and the myristoyl are strong while histidine protonation weakens the native protein-myristoyl interactions with respect to the rest of the native interactions in the protein, and that this combination leads to the intermediate position of the myristoyl group relative to the protein.

We used molecular-dynamics simulations of the folded state for WT, F6L/I85L/I93L, and I85L to assess the extent of burial of the myristoyl group in the protein binding pocket by measuring the distance from the tip of the myristoyl to the bottom of the barrel. We also calculated the time for the position of the myristoyl group in the protein to become decorrelated, which provides a measure of myristoyl dynamics. The simulations suggest that WT accesses both the sequestered and partially accessible states (states I and II). In contrast, F6L/I85L/I93L is predominantly in a sequestered state (state I), with the myristoyl inserted further into the protein than in WT and little fluctuation of the myristoyl into the accessible state (state II). On the other hand, in I85L the myristoyl may be slightly less buried than in WT, with increased population of the accessible state (state II). In addition, the triple mutant transitions between states more slowly than WT based on increased decorrelation time for the position of the myristoyl group compared to WT, whereas the single mutant shows the opposite behavior, transitioning more rapidly with a shorter decorrelation time (Fig. 4*D*). Thus, both the location and dynamics of the myristoyl group in the atomistic simulations are consistent with the experimental energetic data (Fig. 3*C*) and folding simulations (Fig. 4 *A*–*C*), which taken together indicate that the myristoyl: (*i*) makes stronger interactions with the protein in F6L/I85L/I93L, causing it to remain in the sequestered state; (*ii*) makes weaker interactions in I85L so that it stays in the accessible state II; and (*iii*) is poised to switch between the two states in WT.

Localized Stability Changes Associated with Myristoyl Switching. We obtained higher-resolution insights into the energetics of switching by further analysis of simulations combined with experimental measurements of amide H/D exchange rates. Full stabilization of the protein occurs only after the myristoyl is switched from the accessible to the sequestered state (transition from state II to state I). We identified 12 residues that become significantly more ordered after the myristoyl is fully inserted into the pocket (Fig. 5*A*, blue). Some of these residues are close in sequence to the myristoyl and may be expected to behave in this way, whereas

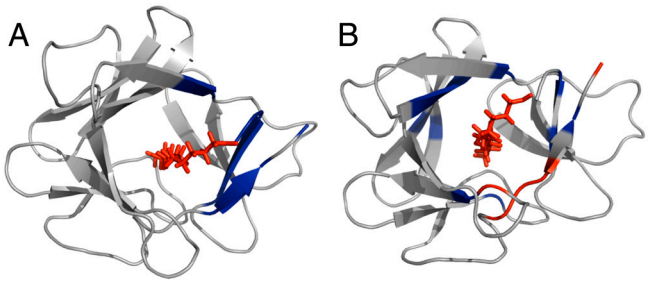

Fig. 5. Changes in dynamics upon myristoylation. (*A*) Top view of hisactophilin with residues predicted to become ordered (blue, G2, N3, R4, A5, F6, K7, H35, V36, E114, E115, I116, I118) upon sequestering of the myristoyl group as observed by coarse-grained simulations. (*B*) Measured change in amide exchange protection factor for myristoylated compared to nonmyristoylated WT hisactophilin, $\Delta P_{\mathrm{pH}\,8.1} = \log(P_{\mathrm{myr}} \cdot P_{\mathrm{non}}^{-1})$ (Fig. S6), at pH 8.1 where the myristoyl group is sequestered. R4, V43, A95, and I116 (blue, Fig. S6) show the largest increase in protection upon myristoylation while other residues are slightly protected (blue); V83, T112, F113, E114, and I118 (red) show decreased protection. The myristoyl group is shown in red stick representations.

others are far in sequence but close in structure. Notably, the N- and C-termini of the protein exhibit the largest increase in order when the myristoyl becomes sequestered.

We obtained an experimental measure of changes in protein flexibility upon myristoylation using amide H/D exchange rate measurements for approximately 35 amides located throughout the protein structure (Fig. 5*B* and Fig. S6*A*). Increased amide H/D protection factors upon myristoylation are observed for many amides throughout the protein, at both pH 5.9 where the protein is predominantly in the accessible myristoyl conformation (state II) and at pH 8.1 where the protein is predominantly in the sequestered conformation (state I) (Fig. S6*A*). This protection is consistent with myristoylation increasing the global protein stability, as has also been observed in chemical denaturation experiments (6, 27). Furthermore, the largest increases in amide protection arising from the myristoyl group from pH 5.9 to 8.1 are observed for amides close to the N- and C-termini (Fig. S6*B*). This is consistent with the increase in structure upon full insertion of the myristoyl group observed by simulation (Fig. 5*A*). The amide protection factors also reveal that a small group of amides (V83, T112, F113, E114, and I118) show small decreases in protection upon myristoylation (Fig. S6*A*). These residues are clustered at one side of the myristoyl binding pocket, suggesting that mobility in this region may be linked to and facilitate switching between accessible and sequestered states.

Conclusions

Post-translational modifications are a common means to regulate protein function. In many cases the regulation is achieved by the modification directly modulating the protein biophysical properties. Our study reveals molecular details of significant changes in protein stability and kinetics caused by myristoylation. The effects of mysristoylation are more pronounced than those observed for glycosylation (5) and ubiquitination (28) and can be simply rationalized by the close interactions of the hydrophobic myristoyl group with its binding pocket, while in the case of glycan and ubiquitin conjugates, the interface with the protein is smaller and dominated by excluded-volume effects. The extensive interface the myristoyl forms with the protein may therefore change the folding enthalpy as well as the protein internal dynamics.

Using a range of complementary experimental and computational approaches, we characterized the pronounced effects of myristoylation on the folding of hisactophilin. The effects on folding cannot be explained solely by the native interactions defined in the NMR structure of hisactophilin with the myristoyl sequestered in its binding pocket (6); additional nonnative hydrophobic

and electrostatic interactions also have significant roles. The coarse-grained simulation models highlight the importance of nonnative hydrophobic interactions in reducing the free energy barrier for folding and stabilizing the protein. The simulations reveal an intermediate state, distinct from the sequestered one observed by NMR and a state with fully exposed myristoyl, where the myristoyl is partially accessible and makes stabilizing nonnative interactions with the protein. In simulations and experiments, hisactophilin has maximal global stability only after the myristoyl switches to the sequestered state. Furthermore, coarse-grained simulations and amide H/D exchange measurements reveal molecular details of switching mechanism involving changes in local stability clustered at one side of the binding pocket and including the N- and C-termini of the protein. The effects of mutating hydrophobic residues distributed around and outside the myristoyl binding pocket reveal the robust effect of myristoylation on folding kinetics, which contrasts with the relative ease of breaking native-state switching. These results suggest that the long and flexible nature of the myristoyl alkyl chain may enable sampling of a relatively broad, nonspecific ensemble of hydrophobic interactions in the transition state that is much more restricted and finely tuned in the native state.

In summary, a combination of computational and experimental approaches provides unique insights on how a common fatty acyl protein modification can tune folding through both native and nonnative interactions, and how changes in stability and dynamics control function. The effects of myristoylation in hisactophilin are similar to results for other proteins where regions of increased local stability are counterbalanced by regions of decreased local stability implicated in function regulation by ligand binding (29–31). The folding energetics and mechanism for myristoylated hisactophilin support the notion that local energetic frustration and the accumulation of strain during switching can be linked to function as observed in allosteric proteins (16) and for functional and/or hydrophobic residues in other proteins (7, 11, 32, 33).

Materials and Methods

Two coarse-grained models of nonnative interactions were used: nonnative hydrophobic interactions modeled by a Guassian potential (13) in which the κ is the hydrophobicity strength, (HPGo model) and nonnative electrostatic interactions modeled by the Debye–Huckel potential (His0 and His1, for high and low pH) (20). Each native interaction is modeled using Lennard–Jones potential with strength of ε. To model nonmyristoylated hisactophilin all the contacts of the myristoyl beads were removed except for the virtual bonds that connect the beads to each other (*SI Materials and Methods*). All-atom molecular dynamics were based on the refined structure of myristoylated hisactophilin and run using the AMBER simulation package (*SI Materials and Methods*). Preparation of hisactophilin variants and measurements of protein stability by equilibrium denaturation curves (23), folding kinetics by stopped flow (24), and amide H/D exchange by NMR (27) were performed as described previously (*SI Materials and Methods*).

ACKNOWLEDGMENTS. We thank Cullen Myers and Dr. Jessica Rumfeldt for stimulating discussions and the University of Waterloo Mass Spectrometry Facility for timely mass-spectrometry analyses. This research was funded by the Natural Sciences and Engineering Research Council of Canada (E.M.M.) and by the Kimmelman Center for Macromolecular Assemblies and the Israel Science Foundation (Y.L.).

1. Onuchic JN, Wolynes PG (2004) Theory of protein folding. *Curr Opin Struct Biol* 14:70–75.
2. Baker D (2000) A surprising simplicity to protein folding. *Nature* 405:39–42.
3. Bryngelson JD, Onuchic JN, Socci ND, Wolynes PG (1995) Funnels, pathways, and the energy landscape of protein folding: A synthesis. *Proteins Struct Funct Genet* 21:167–195.
4. Levy Y, Cho SS, Onuchic JN, Wolynes PG (2005) A survey of flexible protein binding mechanisms and their transition states using native topology-based energy landscapes. *J Mol Biol* 346:1121–1145.
5. Shental-Bechor D, Levy Y (2008) Effect of glycosylation on protein folding: A close look at thermodynamic stabilization. *Proc Natl Acad Sci USA* 105:8256–8261.
6. Smith MT, Meissner J, Esmonde S, Wong HJ, Meiering EM (2010) Energetics and mechanisms of folding and flipping the myristoyl switch in the {beta}-trefoil protein, hisactophilin. *Proc Natl Acad Sci USA* 107:20952–20957.
7. Capaldi AP, Kleanthous C, Radford SE (2002) Im7 folding mechanism: Misfolding on a path to the native state. *Nat Struct Biol* 9:209–216.
8. Sutto L, Latzer J, Hegler JA, Ferreiro DU, Wolynes PG (2007) Consequences of localized frustration for the folding mechanism of the IM7 protein. *Proc Natl Acad Sci USA* 104:19825–19830.
9. Shea JE, Onuchic JN, Brooks CL (1999) Exploring the origins of topological frustration: Design of a minimally frustrated model of fragment B of protein A. *Proc Natl Acad Sci USA* 96:12512–12517.
10. Li L, Mirny LA, Shakhnovich EI (2000) Kinetics, thermodynamics, and evolution of nonnative interactions in a protein folding nucleus. *Nat Struct Biol* 7:336–342.
11. Di Nardo AA, et al. (2004) Dramatic acceleration of protein folding by stabilization of a nonnative backbone conformation. *Proc Natl Acad Sci USA* 101:7954–7959.
12. Clementi C, Plotkin S (2004) The effects of nonnative interactions on protein folding rates: Theory and simulation. *Protein Sci* 13:1750–1766.
13. Zarrine-Afsar A, et al. (2008) Theoretical and experimental demonstration of the importance of specific nonnative interactions in protein folding. *Proc Natl Acad Sci USA* 105:9999–10004.
14. Zhang Z, Chan HS (2010) Competition between native topology and nonnative interactions in simple and complex folding kinetics of natural and designed proteins. *Proc Natl Acad Sci USA* 107:2920–2925.
15. Gosavi S, Chavez LL, Jennings PA, Onuchic JN (2006) Topological frustration and the folding of interleukin-1 beta. *J Mol Biol* 357:986–996.
16. Ferreiro DU, Hegler JA, Komives EA, Wolynes PG (2011) On the role of frustration in the energy landscapes of allosteric proteins. *Proc Natl Acad Sci USA* 108:3499–3503.
17. Capraro DT, Roy M, Onuchic JN, Gosavi S, Jennings PA (2012) Beta-bulge triggers route-switching on the functional landscape of interleukin-1 beta. *Proc Natl Acad Sci USA* 109:1490–1493.
18. Cho JH, Sato S, Horng JC, Anil B, Raleigh DP (2008) Electrostatic interactions in the denatured state ensemble: Their effect upon protein folding and protein stability. *Arch Biochem Biophys* 469:20–28.
19. Weinkam P, Pletneva EV, Gray HB, Winkler JR, Wolynes PG (2009) Electrostatic effects on funneled landscapes and structural diversity in denatured protein ensembles. *Proc Natl Acad Sci USA* 106:1796–1801.
20. Azia A, Levy Y (2009) Nonnative electrostatic interactions can modulate protein folding: Molecular dynamics with a grain of salt. *J Mol Biol* 393:527–542.
21. Thirumalai D, Hyeon C (2005) RNA and protein folding: Common themes and variations. *Biochemistry* 44:4957–4970.
22. Resh M (2006) Trafficking and signaling by fatty-acylated and prenylated proteins. *Nat Chem Biol* 2:584–590.
23. Liu C, et al. (2001) Thermodynamics of denaturation of hisactophilin, a beta-trefoil protein. *Biochemistry* 40:3817–3827.
24. Liu C, Gaspar JA, Wong HJ, Meiering EM (2002) Conserved and nonconserved features of the folding pathway of hisactophilin, a beta-trefoil protein. *Protein Sci* 11:669–679.
25. Smith MT, Mackenzie DW, Meiering EM (2011) Dissecting the molecular determinants of ligand-binding-induced macromolecular switching using thermodynamic cycles. *Protein Eng Des Sel* 24:213–217.
26. Biyun S, Cho S, Thirumalai D (2011) Folding of human telomerase RNA pseudoknot using ion-jump and temperature-quench simulations. *J Am Chem Soc* 133:20634–20643.
27. Houliston RS, Liu C, Singh LM, Meiering EM (2002) pH and urea dependence of amide hydrogen-deuterium exchange rates in the beta-trefoil protein hisactophilin. *Biochemistry* 41:1182–1194.
28. Hagai T, Levy Y (2010) Ubiquitin not only serves as a tag but also assists degradation by inducing protein unfolding. *Proc Natl Acad Sci USA* 107:2001–2006.
29. Namanja AT, et al. (2011) Stereospecific gating of functional motions in Pin1. *Proc Natl Acad Sci USA* 108:12289–12294.
30. Marlow MS, Dogan J, Frederick KK, Valentine KG, Wand AJ (2010) The role of conformational entropy in molecular recognition by calmodulin. *Nat Chem Biol* 6:352–358.
31. Tzeng S-R, Kalodimos CG (2011) Protein dynamics and allostery: An NMR view. *Curr Opin Struct Biol* 21:62–67.
32. Wensley BG, et al. (2010) Experimental evidence for a frustrated energy landscape in a three-helix-bundle protein family. *Nature* 463:685–688.
33. Friel CT, Smith DA, Vendruscolo M, Gsponer J, Radford SE (2009) The mechanism of folding of Im7 reveals competition between functional and kinetic evolutionary constraints. *Nat Struct Mol Biol* 16:318–324.